#### **ORIGINAL ARTICLE**



# A customizable, low-cost alternative for distributed 2D flow sensing in swarms

Jack A. Defay<sup>1</sup> · Jacob M. Peters<sup>1</sup> · Kirstin H. Petersen<sup>1</sup>

Received: 28 August 2021 / Accepted: 4 March 2022 / Published online: 3 May 2022 © International Society of Artificial Life and Robotics (ISAROB) 2022

#### **Abstract**

Many collective behaviors in social insects are mediated by airflow, such as honeybees fanning their wings to drive nest ventilation or to disperse pheromones during olfactory search and aggregation. Empirical investigations of how the local sensing and actuation of individual insects scale up to produce such large scale flows require distributed flow measurement techniques. Common vision-based techniques, however, are not workable in the cluttered dynamic environments in which these social insects live and behave. Here, we developed a customizable, low-cost 2D flow sensor that can measure both magnitude and direction and be deployed in dense sensor arrays on experimental surfaces. While many 2D thermal flow sensor designs have been published, our minimal design uses off-the-shelf components and standard fabrication techniques that should be accessible to most research groups. Here we report on the design and performance of our sensor and provide a user-friendly calibration protocol. The sensor has a measurement range of 0–2 m/s with accuracy of 0.1 m/s, angular resolution of 15°, and a time constant of 3 s. We also discuss modifications that can be made to tune sensor performance for a given application.

**Keywords** Social insects · Flow sensing · Field instruments · Distributed sensing · Wind tunnel

### 1 Introduction

Social insects coordinate collective behaviors through interactions among individuals which sense and modify their local environment. This phenomenon is especially apparent in termite and ant nest construction where extraction and deposition of material in the environment by one individual informs the behavior of others [1]; techniques which have also inspired numerous multi-robot systems [2]. In some cases, coordination arises from distributed interactions with dynamic media, such as airflow, rather than static media. For instance, some termites and ants build and continuously

This work was presented in part at the joint symposium with the 15th International Symposium on Distributed Autonomous Robotic Systems 2021 and the 4th International Symposium on Swarm Behavior and Bio-Inspired Robotics 2021 (Online, June 1–4, 2021).

☐ Jacob M. Peters jmp547@cornell.edu

Kirstin H. Petersen kirstin@cornell.edu

Electrical and Computer Engineering, Cornell University, Ithaca, NY, USA remodel their nests to promote ventilation, and honeybees drive airflow through wing-fanning to drive nest ventilation or to disperse pheromones during olfactory search and aggregation [3–5]. Insights on such flow-mediated coordination can inspire radically new robot coordination algorithms, beyond the stigmergic approach which has been shown in static environments. Empirical study of how the local sensing and actuation of individual insects scale up to produce large scale flows requires distributed flow measurement techniques in cluttered environments in which vision-based flow measurements (e.g., particle image velocimetry) fail. Therefore, we developed a customizable, 2D flow sensor that can be deployed in dense arrays to quantify the flow that is sensed and/or driven by social insects.

Traditional hotwire anemometers are relatively expensive (hundreds of USD) and measure only flow speed, not direction. Microflowns are suitable only for 1D applications such as flow measurement in tubes, e.g. for measuring ventilatory flows in termite mounds [6]. As an alternative, many 2D thermal flow sensors have been published in the last few decades [7–14]. Most of them involve heating elements surrounded by multiple temperature sensors [11], which permit sensing of both magnitude and direction of the airflow along the sensor surface. However, these sensors are produced with



micro-machining or lamination techniques that are inaccessible to nonspecialists and often require complex processing or machine learning to interpret the output [12].

We took inspiration from these sensors, but optimized our design for measurements of directional flows in relation to social insects, including: (1) small and symmetric form factor to minimally affect the existing airflow and insect behavior; (2) robustness to insect interaction; (3) low thermal capacity to support higher temporal resolution; (4) low cost to support large numbers; (5) simple fabrication, customization, and calibration that does not require specialized equipment or know-how; and (6) simple data analysis that can run on commodity computers without specialized software. Our design uses a flexible printed circuit board (PCB) with one central heating element surrounded by 5 thermistors (Fig. 1). Our approach achieves reasonable accuracy of 0.1 m/s, resolution down to 0.3 m/s and 15°, and a time constant of 3 s. The design uses standard PCB fabrication, few components, requires less than 2 h of assembly time, and cost only 13.75 USD, although bulk pricing can reduce the price total substantially. We report on the design and performance of our sensor, detail a calibration protocol that can be implemented by any user in a standard laboratory, and suggest easy customization to suit particular applications. All design files are available open source (https://github. com/CEI-lab/Scalable2DFlowSensor/).

# 2 Design and fabrication

Towards a small, symmetric form factor with low thermal capacity, we implemented the entire sensor on a flexible PCB (Fig. 1A) that can fold along a flexure line such that only the sensing components are exposed and the remainder can be slotted through the experimental surface where it can be accessed and wired from below. We ordered these PCBs from OSHpark at 3.66 USD per piece.

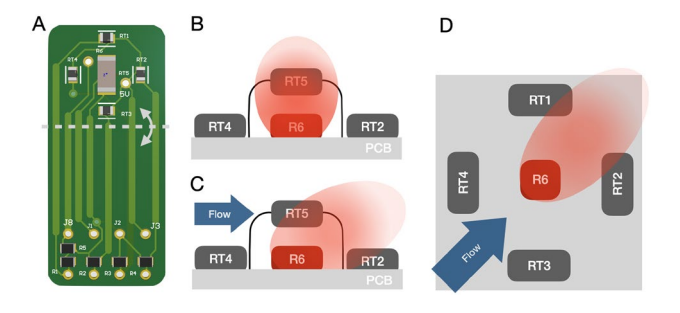


**Fig. 1 A** Sensor PCB. The dashed line indicates a fold line. Four thermistors (RT1–4) surround a heated resistor (R6); an additional through-hole thermistor (RT5) is suspended directly above R6. **B** At zero airspeed, the heat generated by R6 rises straight up to heat RT5. **C**, **D** At higher airspeeds, the heat is biased towards a subset of RT1–RT4 which indicates the direction of airflow

The sensor is composed of a heating element surrounded by 4 thermistors to measure the direction of the airflow and an additional thermistor suspended above the heating element by 2 mm to measure airspeed (Fig. 1B–D). We chose to decouple these measurements in hardware, rather than software as has been shown in related work, to thermally isolate the sensor from the PCB. This improves response time and simplifies data analysis. Our heating element is a  $100\Omega$  2W 2010 surface mount (SMD) power resistor from TE Connectivity. This resistor acts as a resistive heater run in constant power (CP) mode, approximated by a constant input voltage, similar to the system shown in [15]. The four surrounding  $10 \text{ k}\Omega$  0805 SMD thermistors are from Vishay. The last  $10 \text{ k}\Omega$  through-hole thermistor is from TDK Electronics (B57541G1103F000).

The thermistors are coupled in series with fixed resistors such that their output can be read using a simple Analog to Digital Converter (ADC). For larger arrays, multiple sensors can be coupled to any embedded processor with a multichannel ADC as is common e.g. in the popular Arduino platforms. We converted the sensor output,  $V_{\rm out}$ , to airspeed using a linearly interpolated lookup table obtained from our calibration curve. To measure airflow direction, we used the Arduino Mega which is capable of differential amplification and conversion. Specifically, we measured differential inputs from opposing (North–South, East–West) thermistors, similar to a Wheatstone Bridge configuration,  $\delta V_{\rm out}^{NS}$  and  $\delta V_{\rm out}^{EW}$ , and used simple trigonometry to compute the angle of the airflow:

$$\phi = \arctan \frac{\delta V_{\text{out}}^{NS}}{\delta V_{\text{out}}^{EW}}$$
 (1)

# 3 Wind tunnel design for sensor calibration

In lieu of more advanced equipment, we detail two simple wind tunnel designs made with readily accessible components for calibrating the magnitude sensor (Fig. 2). The first produces flow up to 2 m/s, the other up to 5.5 m/s. Our design balances constraints of expense, airspeed range, and laminar flow.

The slow wind tunnel consists of a main stage ( $140 \times 140 \times 600 \text{ mm}^3$ ) with a computer fan (213 cfm, Wathai B07SGWNV5J) drawing air out from the tunnel at one end, and a straw-based laminarizer at the other end. The faster wind tunnel has the same length, but a smaller cross-section ( $50 \times 50 \text{ mm}^2$ ) and an additional settling chamber and linear compression stage ( $140 \times 140 \times 254 \text{ mm}^3$ ) mounted before the fan. To induce laminar flow, we use a long main stage, a  $10^\circ$  compression stage transition angle, and a straw



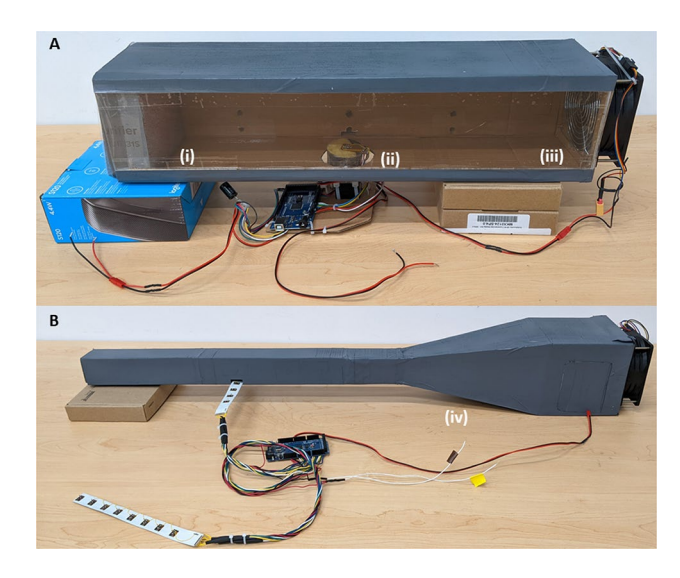


**Fig. 2** A Windtunnel with airspeeds of 0–2 m/s with a straw-based laminarizer (i), a sensor (ii), and a fan (iii). **B** Windtunnel with compression stage (iv) and airspeeds of 0–5.5 m/s. Note that the sensor in A is mounted on a turntable that was flush with the surface during calibration. It is raised for visibility in this figure

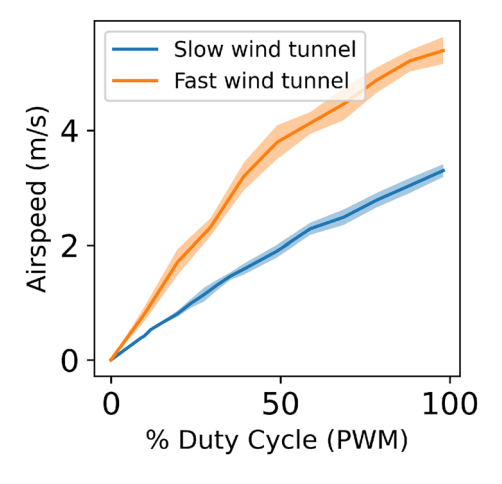


**Fig. 3** Calibration curves for the windtunnels. The *x*-axis shows the fan duty cycle, the *y*-axis shows the airspeed measured with a commercial anemometer (TSI 9535 Velocicalc Digital Air Velocity Meter). The solid line denotes the average over 60 s (600 samples) and the shaded region shows the standard error

length to diameter ratio of 10. The tunnels were made out of cardboard with a slot near the floor to insert the sensors. The straws were kept in place by a plastic wire mesh, and we found that additional layers of mesh could be added to extend the lower range of active airspeeds below 0.5 m/s. We also added an optional viewing window along the side of the tunnel made of acrylic.

We characterized the wind tunnel at the height of interest for flow generated by scent-fanning bees (i.e., approximately 3 mm above the surface) using a reference anemometer

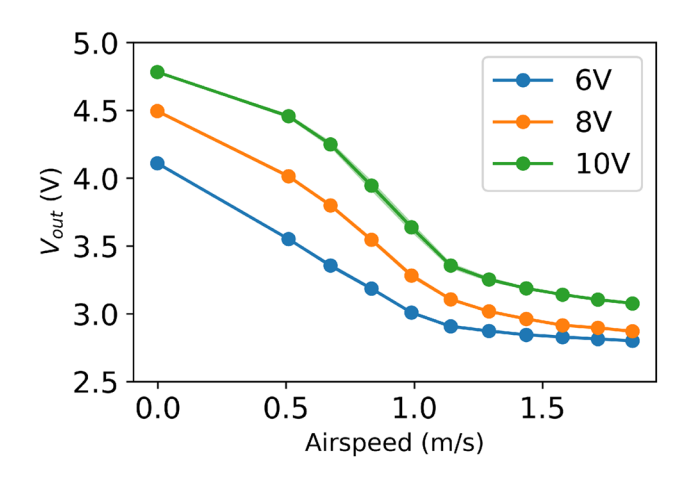
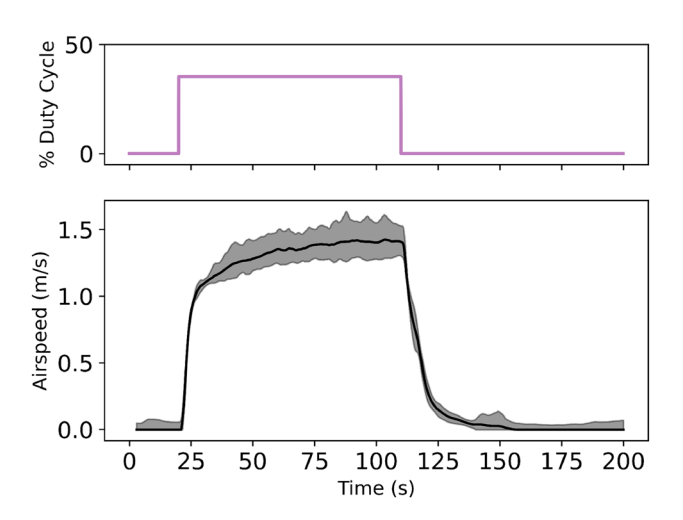


Fig. 4 Magnitude calibration curve at different driving voltages



**Fig. 5** Example of a step performed in the wind tunnel, with corresponding response from the magnitude thermistor (RT5)

(Fig. 3). We then used the wind tunnel to calibrate our sensors at the same height. To calibrate the magnitude sensor, we ran the fan at various duty cycles in 60 s intervals while recording  $V_{\rm out}$ . Figure 4 shows calibration data for three different supply voltages across the power resistor.

## 4 Sensor characterization

To characterize the sensor, we considered four key metrics: accuracy, range, measurement resolution, and temporal resolution. The range of the magnitude sensor is shown in Fig. 4 as a function of the heating element supply voltage. We found that at speeds greater than 2 m/s, the noise in the signal made the readings indistinguishable. Figure 5 shows a step response test from 0 to 2 m/s to characterize the magnitude sensor's time constant. Upon heating,



the sensor has a 90% rise time of 11.00 s, and reaches 63.2% of its final value in 3.01 s. Upon cooling (going from higher to lower airspeed) the time constant is slightly slower: 13.76 s and 6.16 s, respectively. We find the accuracy of the magnitude sensor at steady state by subtracting the calibrated sensor value from known airspeed, for an average and standard deviation error of  $0.11 \pm 0.01$ m/s. To find the sensor resolution, we repeated the step response for incrementally smaller step values (Fig. 6), starting at the middle of the sensor range (1.14 m/s). We consider the minimum resolution to be at the point when the standard deviation at steady state before and during the step overlaps. With a moving average similar to our time constant ( $t_{avg} = 3$  s), the resolution is 0.25 m/s. At  $t_{avg} = 10$ s the resolution improves to 0.1 m/s at the cost of a slower response. In comparison, the ~ 1 K USD anemometer used to calibrate the wind tunnel has a time constant of 1 s and a resolution of 0.01 m/s.

To characterize the directional sensor, we performed similar step response tests (Fig. 7, 8), but with angle. When rotating the sensor from  $0^{\circ}$  to  $50^{\circ}$  relative to the oncoming flow, we found a 90% rise time of 4.3 s. W found the measurement resolution to be 15° with  $t_{\rm avg}=3$  s. At 1.14 m/s airspeed, we found the average and standard deviation error to be  $3.88^{\circ} \pm 0.30^{\circ}$ . We expect that better tuning of the wind tunnel for laminar flow, suppression of 60 Hz interference, and increased differential amplification may improve these numbers.

In Table 1, we compare the performance of this sensor to other 2D sensors reported in literature.

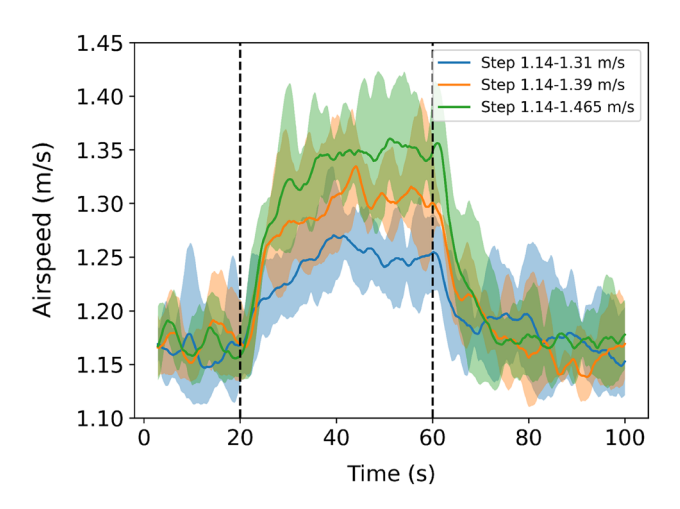


**Fig. 6** Step response performed to determine sensor resolution near the middle of its absolute range (1.14 m/s). Each trial was collected using a 3 s moving average filter. Solid line shows average; shaded region shows standard deviation

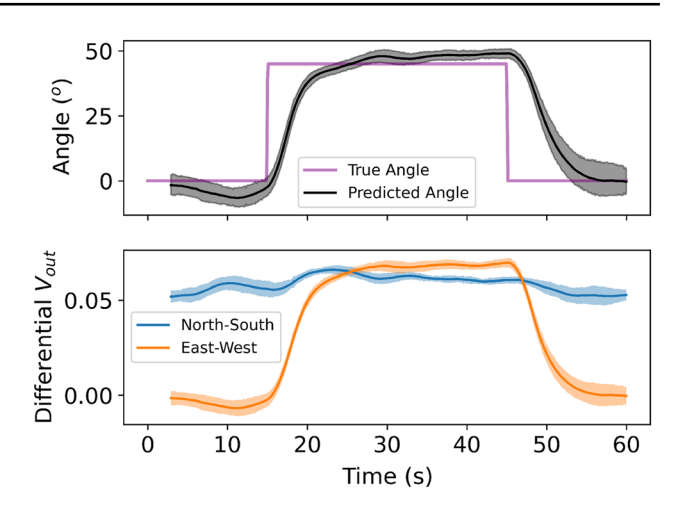


Fig. 7 Computed (top) and raw (bottom) sensor output on angular step response

### 5 Customization

The inherent advantage of the minimalistic design we present here is the ease of customization for different applications. Next, we discuss potential parameters to be changed and how these trade off sensor performance.

There are several ways to change the sensor response time to fit the particular signal to be measured. The sensor is based on a flexible PCB, which is thin, has low thermal mass, and can sit flush with the experimental surface. Flexible PCBs, however, are also more fragile. We found that sensors implemented on stiff 0.8 mm PCB are more robust, but also react slower and transmit the heat over a larger surface which may deter close operation with insects. The thermistors used in our sensor have a thermal mass that is dependent on the size of the glass bead which surrounds

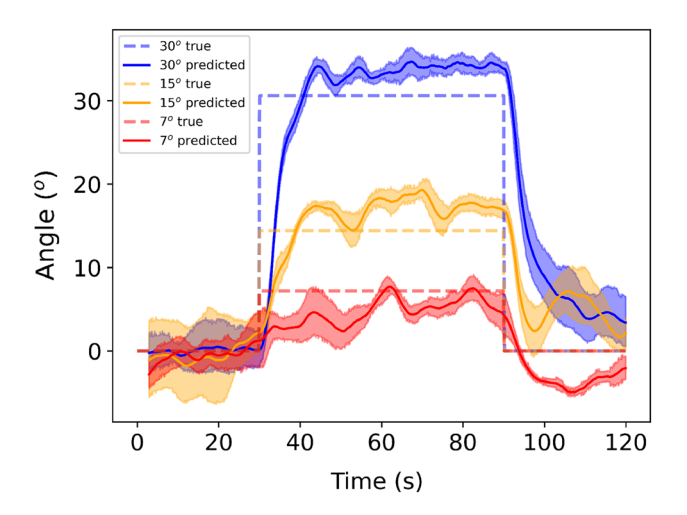


Fig. 8 Angular step response to determine directional resolution, set up similar to Fig. 6



References	Range (m/s)	Magnitude		Direction		Manufacturing
		Accuracy (m/s)	Resolution (m/s)	Accuracy (°)	Resolution (°)	
This paper	2	0.1	0.25	4	15	Std. soldering
[8]	30	0.65	NA	0.96	NA	MEMS
[10]	40	0.5	NA	2	NA	MEMS
[11]	33	0.33	0.04	1.5	1	MEMS
[14]	37	0.5	NA	2.7	NA	MEMS
[16]	10	0.36	NA	1.2	NA	MEMS

Table 1 Key aspects of our sensor compared to other custom sensors in literature

Note that characterization techniques differ between papers

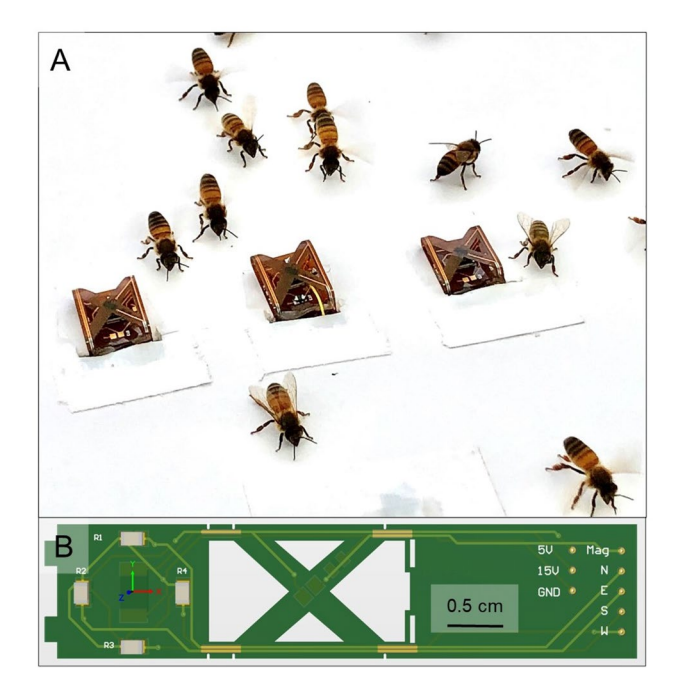


**Fig. 9** A, B Covered sensor designed for measuring airflow driven by scent-fanning honeybees. The bees with their abdomens raised are fanning their wings, driving airflow along the surface (from bottom right to upper left), and seeding the air with pheromone to orient other bees toward the queen. Other bees are walking upstream following this signal

the sensor. We tested a larger bead size (MF58, Uxcell) and found that the small thermistor bead was more responsive and pick up higher frequency fluctuations while the large thermistor bead have a slower response time; specifically, we measured the rise time constant in this setup to be 11.6 s.

To change the absolute range of the sensor, the user can change the the distance of the thermistors to the heating element and the size of the thermistor bead. Another easier modification is to increase the range by increasing the supply voltage for the heating element (R6) at the cost of increased temperature, which may negatively affect nearby insects. Note that excessive heating above 150 °C may also negatively affect the life time of the sensor.

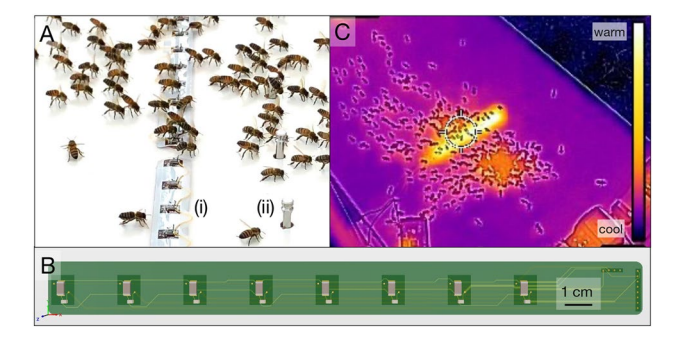


Fig. 10 A, B Magnitude array sensor used in a different honeybee experiment. Our sensor (i) has a low profile relative to the commercial anemometer (ii; TSI 9535) used as a reference. C Thermal image of bees crossing the magnitude sensor array. The bees do not appear to be deterred by the heat generated. The color scale represents relative temperature only. The thermal camera could not supply accurate absolute temperature readings in variable outdoor lighting conditions

To demonstrate the versatility of our approach, we implemented and briefly field-tested two variants. The first variant was designed to better withstand direct insect interactions. We extended the flexible PCB, folding it over three times to produce a stable rectangular cross-section. The roof of this cross-section was slotted as to not hinder airflow. This design permitted us to replace the through-hole thermistor with a cheaper SMD thermistor (Fig. 9). As before, the end of the PCB was slotted through a cavity in the experimental surface. The second variant was a 1D magnitude sensor array with 8 thermistor heating element pairs (Fig. 10A, B). 1D sensing reduced complexity and allowed for more data collection in the brief field season we had.

## 6 Exploratory field test

Our design was motivated by the study of olfactory search and aggregation, used in swarm cluster formation in honeybees (FigS. 9, 10). In the spring and summer, honeybee colonies reproduce through colony fission, a process in which about half of the workers (approximately 10,000 bees) fly from the



nest and land on a nearby surface in the environment (e.g., a tree branch) where they must aggregate around the queen. During this aggregation behavior, worker bees localize and navigate toward the queen by collectively driving pheromone-laden airflow. Some workers grip the surface and fan their wings driving air away from the queen's position to generate a pheromone plume while others walk upstream toward the queen guided by this pheromone plume [5, 17]. We staged this aggregation behavior on a  $0.6 \,\mathrm{m} \times 1.2 \,\mathrm{m}$  board by placing 500 workers from a swarm on one side of the board and a caged queen at the other. We mounted our sensors on the board between the workers and the queen to measure the airflow generated by the honeybees along the surface as they navigated toward the queen.

To test the field-readiness of our sensor, we installed two prototypes on the surface to measure the flows induced by honeybees. We placed two of the magnitude sensor arrays (described above) together to make a 16-sensor array perpendicular to the direction of bee/air movement (Fig. 10B). The bees traversed the sensor array while performing typical scent-fanning behavior, enabling biological measurements which will be the subject of future research. The bees avoided making direct contact with the heating element on the sensor, but because the heating elements are relatively sparse, it did not affect the aggregation process. We also tested the variant of the 2D flow sensor (Fig. 9) with the folded housing which prevented the bees from directly contacting the sensing components.

We validated that the heating elements produced enough heat ( $\sim$  87 °C) to sense effectively from 0 to 2 m/s (Fig. 10C), while the sensors were small and cool enough to not deter honeybees from traversing them (Figs. 9A, 10A). While some characteristics of our sensor were sufficient for our study (i.e., 0.25 m/s resolution; 15° angular resolution, 3 s time constant), the peak airspeed generated by the bees exceeded the 2 m/s limit of our sensor. In future iterations, we intend to increase the range of our sensor by tuning the proximity of the magnitude thermistor to the heating element.

### 7 Conclusion

In brief, we presented a simple method to create and calibrate low cost 2D flow sensors. Although the sensors cannot compare in performance to those made with more complex manufacturing techniques, they lend themselves to easy customization for large scale deployment with social insects. This work to create accessible technology is an important step in the process of uncovering how social insects sense, manipulate, and coordinate through airflow.

Acknowledgements This work was supported by a National Science Foundation (NSF) Award (#1739671), a Cornell Louis Stokes Alliance for Minority Participation (LSAMP) Award, and the Packard Fellowship for Science and Engineering.

#### References

- Perna A, Theraulaz G (2017) When social behaviour is moulded in clay: on growth and form of social insect nests. J Exp Biol 220(1):83. https://doi.org/10.1242/jeb.143347
- Petersen K, Nagpal R (2017) Complex design by simple robots: a collective embodied intelligence approach to construction. Arch Des 87(4):44
- 3. Peters JM, Gravish N, Combes SA (2017) Wings as impellers: honey bees co-opt flight system to induce nest ventilation and disperse pheromones. J Exp Biol 220(12):2203. https://doi.org/10.1242/jeb.149476
- Peters JM, Peleg O, Mahadevan L (2019) Collective ventilation in honeybee nests. J R Soc Interface 16(150):20180561. https:// doi.org/10.1098/rsif.2018.0561
- Peters JM, Petersen KH (2020) Honeybee swarms use a flowmediated pheromone signaling scheme to coordinate aggregation. SICB 60:E185–E185
- King H, Ocko S, Mahadevan L (2015) Termite mounds harness diurnal temperature oscillations for ventilation. Proc Natl Acad Sci 112(37):11589. https://doi.org/10.1073/pnas.1423242112
- Zhu Y, Chen B, Qin M, Huang Q (2014) 2-D micromachined thermal wind sensors—a review. IEEE Internet Things J 1(3):216. https://doi.org/10.1109/JIOT.2014.2319296
- Que R, Zhu R (2015) A compact flexible thermal flow sensor for detecting two-dimensional flow vector. IEEE Sens J 15(3):1931. https://doi.org/10.1109/JSEN.2014.2367017
- Zhu R, Que R, Liu P (2017) Flexible micro flow sensor for micro aerial vehicles. Front Mech Eng 12(4):539. https://doi.org/10. 1007/s11465-017-0427-0
- Wang S, Yi Z, Qin M, Huang Q (2018) A 2D wind sensor using the ΔP thermal feedback control. J Microelectromech Syst 27(3):377. https://doi.org/10.1109/JMEMS.2018.2812805
- Ye Y, Yi Z, Gao S, Qin M, Huang Q (2018) Octagon-shaped 2-D micromachined thermal wind sensor for high-accurate applications. J Microelectromech Syst 27(4):739. https://doi.org/10.1109/ JMEMS.2018.2849086
- Barmpakos D, Famelis IT, Moschos A, Marinatos D, Kaltsas G (2019) Design and evaluation of a multidirectional thermal flow sensor on flexible substrate. J Sens. https://doi.org/10.1155/2019/8476489
- Gao S, Yi Z, Ye Y, Qin M, Huang Q (2019) Temperature effect and its compensation of a micromachined 2-D anemometer. IEEE Sens J 19(14):5454. https://doi.org/10.1109/JSEN.2019.2906192
- Lan Y, Zou Y, Ma X, Shi Y, Fan J, Hai Y, Wang X, Yang J, Feng Q (2020) Fabrication and characterization of dual coordinate self examined thermal flow sensor arrays based on longitudinal heat conduction. IEEE Sens J 20(1):434. https://doi.org/10.1109/JSEN. 2019.2941531
- Shen G, Qin M, Huang Q (2010) A cross-type thermal wind sensor with self-testing function. IEEE Sens J 10(2):340. https://doi.org/10.1109/JSEN.2009.2034625
- Liu H, Lin N, Pan S, Miao J, Norford LK (2013) High sensitivity, miniature, full 2-D anemometer based on MEMS hot-film sensors. IEEE Sens J 13(5):1914. https://doi.org/10.1109/JSEN.2012. 2236014
- Nguyen DMT, Iuzzolino ML, Mankel A, Bozek K, Stephens GJ, Peleg O (2021) Flow-mediated olfactory communication in honeybee swarms. Proc Natl Acad Sci 118(13): e2011916118. https:// doi.org/10.1073/pnas.2011916118

**Publisher's Note** Springer Nature remains neutral with regard to jurisdictional claims in published maps and institutional affiliations.

